Mon. Not. R. Astron. Soc. **000**, 1–12 () Printed 16 May 2008 (MN LATEX style file v2.2)

Finding how many isolating integrals of motion an orbit obeys

D. D. Carpintero[1,2⋆]
[1]*Fac. de Cs. Astronómicas y Geofísicas, Univ. Nac. de La Plata, Paseo del Bosque S/N, 1900 La Plata, Argentina*
[2]*Instituto de Astrofísica de La Plata, CCT La Plata - CONICET/UNLP, Argentina*

arXiv:0805.2532v1 [astro-ph] 16 May 2008

ABSTRACT

The correlation dimension, that is, the dimension obtained by computing the correlation function of pairs of points of a trajectory in phase space, is a numerical technique introduced in the field of nonlinear dynamics in order to compute the dimension of the manifold in which an orbit moves, without the need of knowing the actual equations of motion that give rise to the trajectory. This technique has been proposed in the past as a method to measure the dimension of stellar orbits in astronomical potentials, i.e., the number of isolating integrals of motion the orbits obey. Although the algorithm can in principle yield that number, some care has to be taken in order to obtain good results. We studied the relevant parameters of the technique, found their optimal values, and tested the validity of the method on a number of potentials previously studied in the literature, using the SALI, Lyapunov exponents and spectral dynamics as gauges.

Key words: stellar dynamics – galaxies: kinematics and dynamics – methods: numerical

1 INTRODUCTION

The characterization of the orbits supported by an astrophysical potential is of interest in order to study self-consistent models of stellar systems. Schwarzschild (1979, 1982), for example, pioneered the construction of steady state distribution functions from a well chosen set of regular orbits belonging to a given potential; other studies followed on the same line (e.g. Cretton, Rix & de Zeeuw 2000). Thus, it was established that regular orbits act as a dynamical skeleton of a stellar system. Moreover, among regular orbits, those that are resonant and stable are of utmost importance, since they generate entire families of orbits around them: they constitute the backbone of the system. On the other hand, chaotic orbits, the existence of which in realistic models of galaxies is nowadays beyond doubt (Valluri & Merritt 1998; Voglis, Kalapotharakos & Stavropoulos 2002; Muzzio, Carpintero & Wachlin 2005), are important to the dynamical evolution of stellar systems. In particular, the slow difusion of many chaotic orbits through their allowed phase space may affect even the global characteristics of the system. As Muzzio (2003) and Muzzio & Mosquera (2004) showed, the spatial distribution of fully chaotic orbits (i.e., those which obey only one isolating integral of the motion) and partially chaotic orbits (those which obey two integrals) is quite different. This points towards a different dynamical role for each type of chaoticity, although what kind of role is still unknown.

Thus, finding regular, resonant, non resonant, partially chaotic and fully chaotic orbits is fundamental in the study of the dynamics of a stellar system. They all are defined by the number of isolating integrals of motion that they obey. For an N-dimensional potential, regular orbits have N or more isolating integrals, whereas chaotic orbits obey less than N isolating integrals[1]. Among regular orbits, those that are not resonant obey exactly N isolating integrals, whereas those resonant have one more isolating integral for each additional resonance. On the other hand, among chaotic orbits, fully and partially chaotic orbits are also distinguished by the number of isolating integrals they have, as said above. Thus, a method allowing to determine the number of isolating integrals an orbit obey is a fundamental tool in studying the dynamics of a stellar system.

One of the main consequences of obeying isolating integrals of motion is the dimension of the manifold on which the orbit moves. Since an isolating integral is, by definition, a non-degenerate[2], time independent funcion of the phase space coordinates the value of which is constant along the orbit, it reduces

[1] A regular orbit, by definition, has N or more isolating integrals of motion. However, a chaotic orbit is defined through its sensitivity to the initial conditions in phase space: if the initial conditions of the orbit are infinitesimally displaced, the distance between the original orbit and the new orbit grows exponentially with time. These definitions do not complement each other. Whereas it can be proved that a regular orbit is not chaotic and a chaotic orbit is not regular (e.g. Jackson 1991, §8.3), it has not been proved that every irregular (i.e. not regular) orbit is chaotic, or, in other words, that every orbit obeying less than N isolating integrals has sensitivity to the initial conditions. Nevertheless, to avoid confusion, we will follow here the widespread convention of considering irregular orbits and chaotic orbits as the same set.

[2] A non-degenetate function takes, at most, a finite or infinite countable

⋆ E-mail: ddc@fcaglp.unlp.edu.ar

in one the dimension of the manifold in which the orbit moves (Binney & Tremaine 2008, §3). Thus, if $N_{\rm ps}$ is the dimension of the phase space, an orbit obeying $N_{\rm i}$ isolating integrals moves in a manifold of dimension $N_{\rm ps} - N_{\rm i}$. One can then ascertain the number of integrals that an orbit obeys by computing the dimension of the space in which it moves. To be brief, we will refer hereafter to 'isolating integrals' as simply 'integrals', and to 'the dimension of the manifold on which an orbit moves' as 'the dimension of an orbit'.

The traditional methods to compute the dimension of an orbit or the number of its integrals are: a) Surfaces of section (e.g. Hénon & Heiles 1964; Contopoulos 1983). As is well known, this method needs a qualitative judgment on a plot, and cannot distinguish between orbits moving in 3 o more dimensions. b) Lyapunov exponents (e.g. Bennetin et al. 1980). This method is the standard tool to separate regular from chaotic orbits; it is quite reliable, and can in principle recognize the dimension of chaotic orbits. On the negative side, since one needs both to integrate a set of variational equations and to integrate along large intervals in order to approximate $t \rightarrow \infty$, it is quite expensive in terms of computing time, and, furthermore, it cannot recognize the dimension of regular orbits. c) Spectral dynamics (e.g. Binney & Spergel 1982; Carpintero & Aguilar 1998). Taking into account that a regular orbit on an N-dimensional potential moves on a manifold diffeomorphic to a N-dimensional torus (Arnold 1989), the natural frequencies of revolution around the N independent circles of the torus must be reflected in the Fourier spectra of the orbit. This allows to find whether there are resonances, and thus the dimension of the orbit can be established. Unfortunately, the method is not suitable for analizing rotating potentials, requires a fine tuning of a set of numerical parameters for each different potential, and cannot find the dimension of chaotic orbits. The frequency map method (Laskar 1990) is based on the same idea. d) The Smaller Alignment Index, or SALI (e.g. Skokos et al. 2004), and its generalization, the Generalized Alignment Index, or GALI (e.g. Skokos, Bountis & Antonopoulos 2007). Both methods are based in a geometrical property of phase space vectors joining close initial conditions, namely that they align themselves or not depending on the geometrical properties of the local dynamics of the system, allowing a fast and accurate determination of whether an orbit is regular or chaotic. The GALI, in particular, although cannot retrieve the dimension of a chaotic orbir, do allow to discern the dimension of the torus of regular orbits, making it an excellent gauge to our results.

Grassberger & Procaccia (1983) have proposed a method to find the dimension of (the attractor of) an orbit in an arbitrary dynamical system, the equations of motion of which are unknown, based on the computation of the correlation integral of the time series of an arbitrary observable. In this context, several improvements have been made to the method (e.g. Dvořák & Klaschka 1990; Ding et al. 1993), and many caveats and spurious estimations have been found (e.g. Kantz & Schreiber 1997). Also, some implementations have been made in the astronomical field (e.g. Heinämäki et al. 1998). The application of the method to find the dimension of an orbit integrated in an astronomical potential, i.e., knowing the equations of motion and being able to sample the actual trajectory of the system at arbitrary points, was first proposed by Carnevali & Santangelo (1984), and more recently by Barnes (2001). The rationale is as follows. Suppose that a given orbit obeys $N_{\rm ps} - 1$ isolating integrals, i.e., it is closed and therefore unidimensional. Given a small hypersphere (in phase space) of radius r around a point P of this orbit, the number of other points of the orbit included into the sphere will grow linearly as r grows. If the orbit obeyed $N_{\rm ps} - 2$ integrals, moving in a bidimensional surface, the number of points would grow as r^2 as r grows. From this point on, it is clear that if the orbit is moving on a D-dimensional space, the number of points would grow as r^D as r grows. This simple mechanism, in principle, allows to easily compute the dimension of the orbit and, therefore, the number of integrals of motion it obeys.

2 THE METHOD AND ITS DRAWBACKS

Carnevali & Santangelo (1984) and Barnes (2001) have developed a simple algorithm in order to compute the dimension D of an orbit following the foregoing idea. Given a set of phase space points of the orbit, first compute the distances between pairs of them. Second, compute the cumulative distribution function of those distances. This is nothing but the correlation integral $C(r)$ of the points of the orbit, i.e., an histogram of the number of pairs of points separated by a given distance or less. This function must be precisely equal to r^D, i.e., the number of pairs closer than a given distance must grow as r^D. Therefore, from a log–log plot of $C(r)$, a straight line can be fitted, its slope giving the desired exponent D which is the dimension sought. A few caveats are in order: a) The exponent D is theoretically obtained only in the limit $r \rightarrow 0$; thus, the slope must be computed avoiding large values of r. b) Unfortunately, since the volume of phase space is proportional to $r^{N_{\rm ps}}$, there will be always few points in the region $r \simeq 0$, so this region of $C(r)$ will be noisy in general, and therefore must be also avoided in computing D. c) In order to avoid autocorrelations, the points of the orbit should not be too close in time; otherwise, $C(r)$ will tend to yield $D = 1$ at short distances (see §3.3). Therefore, in order to build up the histogram, the distances should be computed only between a random subsample of the integrated points. Of course, the number of points $N_{\rm p}$ of the orbit must be sufficient so as to get a reasonable good computation of $C(r)$.

As described, the method is very simple indeed. Carnevali & Santangelo (1984) and Barnes (2001) give several examples of its application to orbits supported by different astronomical potentials, and the results seem encouraging. However, in order to compete against other methods, the algorithm must be capable of classify orbits blindly; otherwise, it would be not better than inspecting surfaces of section. To see whether it is the case, we choose a Stäckel potential, for it has all its orbits regular (i.e., they all must have $D = 3$, with the possible exception of a few orbits with $D = 2$), and therefore we know the correct outcome beforehand, allowing us to assess immediately how good is the method, at least in this particular case. Thus, we integrated 5487 orbits in the potential generated by the perfect ellipsoid density distribution

$$\rho(\boldsymbol{r}) = \frac{\rho_0}{(1+m^2)^2}, \tag{1}$$

where

$$m^2 = \frac{x^2}{a^2} + \frac{y^2}{b^2} + \frac{z^2}{c^2}, \tag{2}$$

and ρ_0, $a \leqslant b \leqslant c < 0$ are constants (de Zeeuw 1985). We used $a = -1$, $b = -0.390625$, $c = -0.25$, and $\pi^2 \rho_0 abc = 1$. The orbits were integrated along 500 periods with a time step of 1/200

number of values for each set of values of its independent variables. This is the condition distinguishing isolating and non isolating integrals of motion.

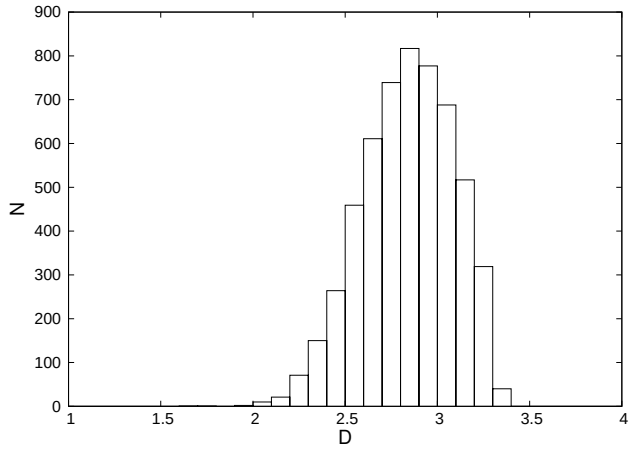

Figure 1. Number of orbits N with dimension D, for 5487 orbits integrated in a Stäckel potential, using 10^4 points out of the 10^5 points of the orbit to compute the correlation integral.

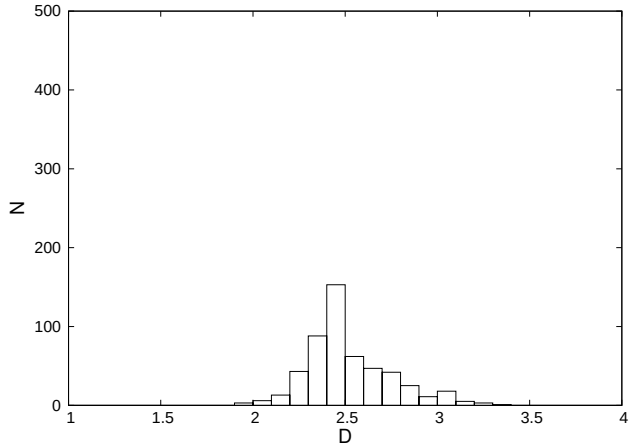

Figure 2. Same as Fig. 1, but only for those orbits that had $D \leqslant 2.5$ in the original classification, and here using 10^5 points out of the 10^6 points of the orbit to compute the correlation integral.

of the respective orbital period, so as to get 100,000 points for each orbit. The dimensions D were computed using the distances of a random sample of 10,000 of those points. The result is shown in Fig. 1, where it can be seen a wide dispersion of values instead of the unique expected value $D = 3$. In order to verify whether the number of points $N_{\rm p}$ was inadequate (Barnes 2001, §4), we took the 520 orbits that lie to the left of $D = 2.5$, and integrated them along 5000 periods, effectively increasing both the number of orbital points and the number of sample points by ten. The result is showed in Fig. 2, where it can be seen again that the orbits do not pile up around $D = 3$. This result, besides showing that a naïve implementation of the method does not yield good results, highlights another point: a non-integer value of D does not necessarily denote a fractal dimension (Carnevali & Santangelo 1984), but may indicate a poor computation of the true dimension.

3 NUMERICAL IMPLEMENTATION

It is clear that a careful numerical implementation of the method is essential to get acceptable results. We have identified several parameters that affect the outcome. To illustrate the analysis, we will use, in the following, two orbits integrated in the Stäckel potential generated by the perfect ellipsoid density distribution (Eq. [1]). Table 1 shows the respective initial conditions. The first orbit is a box orbit; the second one is a z–tube orbit; both orbits move in a manifold of dimension $D = 3$. Also, in all cases the function $C(r)$ has been normalized to its maximum value, that is, $C(r) = 1$ at large distances.

Table 1. Initial conditions of the example orbits.

	Box	z–tube
x	1.163562178611755	0.5087397098541260
y	−0.8299766778945923	−1.472079634666443
z	0.06499148160219193	0.8406194448471069
v_x	0.2304639220237732	0.4684486091136932
v_y	0.1688854843378067	0.01424702629446983
v_z	−0.04289411380887032	−0.1927715390920639

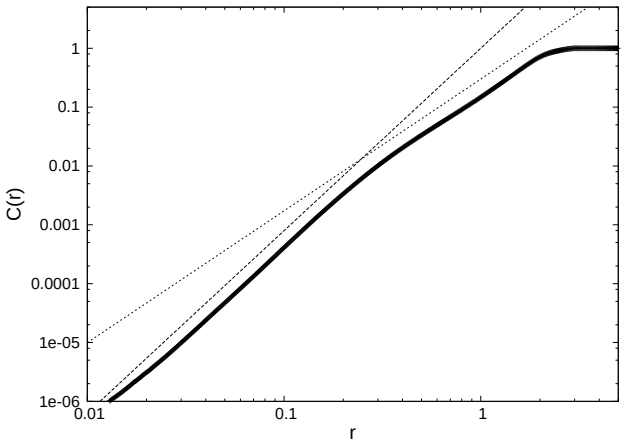

Figure 3. Correlation integral $C(r)$ of the box orbit. The straight lines have slopes 3.10 and 2.24, respectively.

3.1 The window

In order to automate the procedure, the portion of $C(r)$ to be used to fit the straight line –the *window*– must not be chosen by eye. We solve the problem by using a mobile window, that is, by computing the slope of $C(r)$ several times, each one using only the points defined by a window of fixed length placed in a different location of the function $C(r)$. In order not to miss any good fitting, the window is placed starting at every computed point of $C(r)$. Also, due to the uncertainty of the slopes computed with too few points, the length of the window has to have a minimum; a window spanning at least a decade in r should suffice (Grassberger & Procaccia 1983). Once the slopes have been computed for each position of the window (using least squares fitting), we choose as the desired slope that with the minimum error. Here we define 'error' as the value of χ^2 yielded by the least squares fitting (Press et al. 1994). But, as Fig. 3 shows, there is still a problem to solve: the correlation integral typically admits two possible slopes, $D = 3.10$ and $D = 2.24$ for the case of the box orbit of the Figure. Fig. 4 shows the error of the fitting as the window was displaced along the function $C(r)$, and the value of the corresponding slope. As can be seen, the error has two minima, corresponding to the two slopes seen by eye.

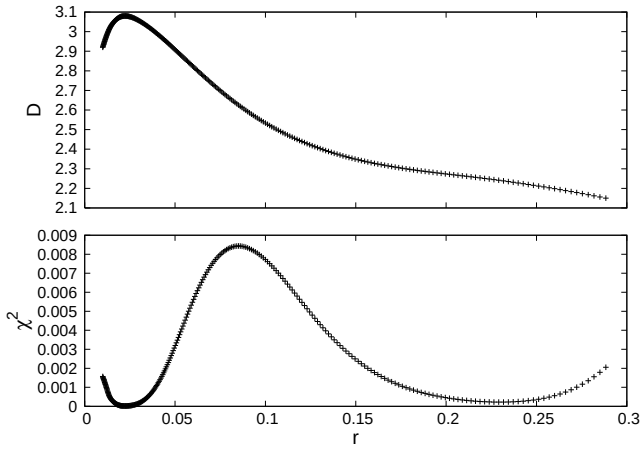

Figure 4. Upper panel: dimension D obtained from least squares fittings to the function $C(r)$ illustrated in Fig. 3. The abscisae of each point corresponds to the starting point of a decade-long window used to obtain the corresponding value of D. Lower panel: the error χ^2 for each value of D. Two minima can be clearly seen; the left one is always chosen to compute D, whenever the neighboring points reach enough height.

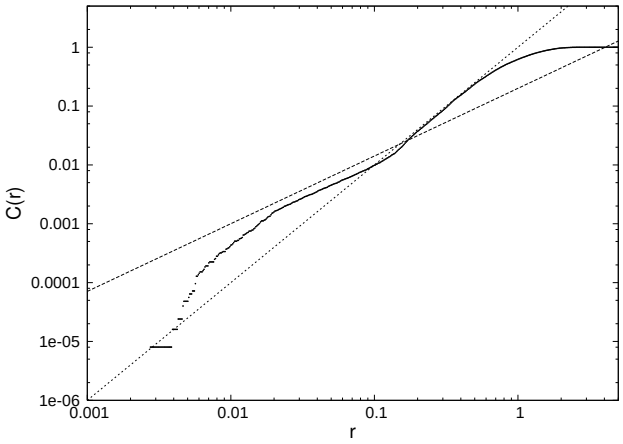

Figure 5. Correlation integral $C(r)$ of an orbit integrated in a Plummer potential $\Phi = -C/\sqrt{r^2 + a^2}$ with $C = 1$ and $a = 0.2945243$. The orbit is a rosette ($D = 2$), but the generating ellipse rotates at a very low angular velocity, and the orbit is seen with $D = 1$ at short distances. The straight lines have slopes 1.15 and 2, respectively.

Which minimum should be chosen? To answer this, it has to be taken into account that the correlation integral gives the dimension of the orbit only at small distances, and, moreover, that at larger values of r, the cumulative function $C(r)$ saturates at two points: a) when all the distances have been incorporated into the histogram ($C(r) = 1$), and b) well before that, when the distances are comparable to the typical diameter of the volume of phase space occupied by the orbit, because there is a lack of points at distances so large. Therefore, it seems safe to claim that the slope with the minimum corresponding to small distances is the correct one. We accomplish this by simply picking up the value of the slope corresponding to the first minimum found when the window is displaced from small values of r towards larger values. In the example, the correct slope $D = 3.1$ is thus chosen.

Nevertheless, there are cases in which the first minimum does not yield the real dimension of the orbit, These include shallow minima indicating a region of low curvature in $C(r)$, giving smaller errors than the surrounding regions, but not being representative of the dimension of the orbit. To avoid choosing these minima, a minimum is taken only if the surrounding values of χ^2 reach at least three times the own value of the minimum. Still, in other cases, the first minimum does not correspond to the true value of D because it is a circumstancial good fitting. Fig. 5 shows one of these cases. In fact, in this example, a longer integration yields $D = 2$, once the orbit begins to cover densely its 2D manifold. Although the abovementioned shallow minimum argument is applicable in many of these cases, there are examples in which it is not. Fig. 6 shows that the first minimum in χ^2 corresponding to the orbit of Fig. 5 is very deep, so the dimension to which it corresponds ($D = 1.15$) will be taken as correct. Since the regions of these first minima often span less than one decade in r, one could shorten the length of the window in order to rise the errors and turn the minima into shallow ones; however, as said before, the shortest acceptable window must span at least one decade in order to achieve good results in the general case. Therefore, orbits that behave like the one described will be missclassified unless they are integrated during longer periods.

As an additional safeguard, the values of $C(r)$ at very small distances are not included in any window, thus avoiding the noisy region, which may introduce spurious 'good' values of D by

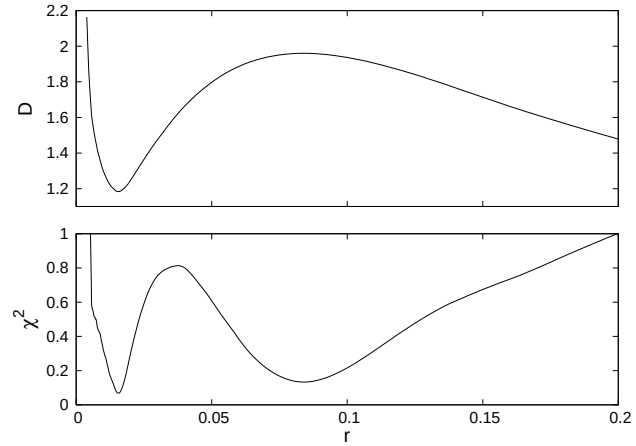

Figure 6. As Fig. 4, but for the orbit of Fig. 5. The first minimum of χ^2 is not shallow.

chance. Since the information about D is contained at small values of r, this cut should be chosen wisely; it should not embrace any valuable region of $C(r)$. We have found that cutting the region $C'(r) < 100$ from the analysis, where $C'(r)$ is the unnormalized correlation integral, effectively avoids the noisy region without affecting the results.

3.2 The number of points to compute distances

The main parameter is, undoubtely, the number of points $N_{\rm p}$ taken from the orbit in order to compute distances among them and thus build up the correlation integral $C(r)$. Let $N_{\rm orb}$ the number of integrated points of the orbit, and let f the fraction of those points used to compute $C(r)$, i.e., $N_{\rm p} = fN_{\rm orb}$. Fig. 7 shows the result of applying several values of f to the z–tube orbit, using $N_{\rm orb} = 300,000$. As can be seen, unless $f < 0.05$ –in which case the autocorrelation of the points of the orbit begins to play a role–, the result is robust enough. Taking into account that the larger is f the more numerically expensive is the computation of $C(r)$, we chose the value $f = 0.1$.

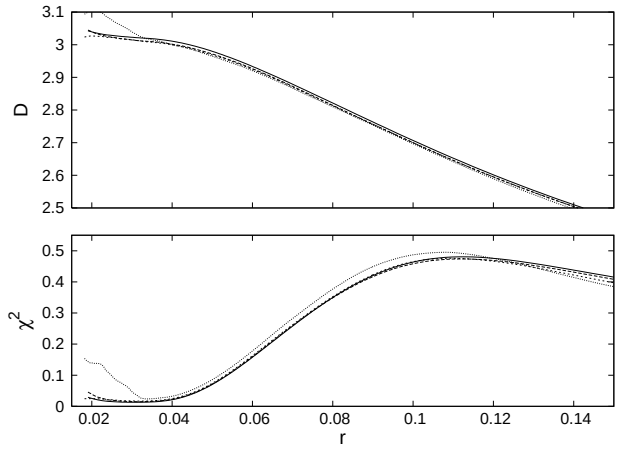

Figure 7. Top: Slopes of the different portions one decade long of the correlation integral of the z–tube orbit when computed with $f = 0.02$ (dotted line), $f = 0.05$ (long dashed line), $f = 0.1$ (solid line) and $f = 0.2$ (short dashed line, almost superimposed over the solid line). Bottom: errors associated with them.

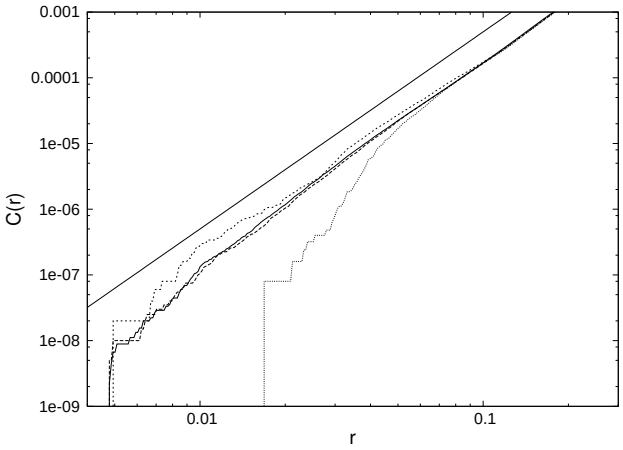

Figure 8. Correlation integral of the z–tube orbit at small distances, computed using different number of points $N_{\rm p}$. A straight line of slope 3 has been added for reference. Dotted line: $N_{\rm p} = 5 \times 10^3$, short-dashed line: $N_{\rm p} = 10^4$, long-dashed line: $N_{\rm p} = 2 \times 10^4$, solid line: $N_{\rm p} = 3 \times 10^4$.

Once f is fixed, there remains the choice of $N_{\rm p}$ –which in turn determines $N_{\rm orb}$ through f. Fig. 8 shows, for the z–tube orbit, the correlation integral at small distances when $N_{\rm p}$ is varied from 5×10^3 to 3×10^4. We can see that this regime of small distances, being the most important, is quite affected by $N_{\rm p}$. Only when $N_{\rm p} \simeq 2 \times 10^4$ the slope is close to 3. Further increases of $N_{\rm p}$ did not improve significantly the result in this example. Fig. 9 shows the respective slopes and errors computed for this case.

In repeating this kind of experiment with other 3D potentials in which chaotic orbits are allowed (the triaxial generalization of the Dehnen potential (Merritt & Fridman 1999) and the numerical potential described below), we found that greater values of $N_{\rm p}$ were required, due to the fact that the number of points needed to cover a 4D or 5D manifold is quite large; we have found that $N_{\rm p} = 5 \times 10^4$ is enough to cope with $D = 5$ orbits (i.e., 5×10^5 orbital points); larger values did not, in general, improve the results. 2D potentials, on the other hand, required fewer points; $N_{\rm p} = 3 \times 10^4$ suffice even for chaotic orbits. Therefore, we adopted $N_{\rm p} = 5 \times 10^4$ for 3D potentials and $N_{\rm p} = 3 \times 10^4$ for 2D potentials.

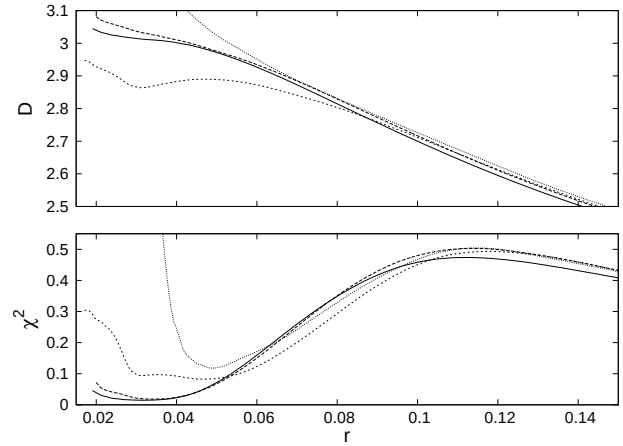

Figure 9. Slopes of the different portions one decade long of the curves in Fig 8, and errors associated with them. Lines as in Fig. 8.

3.3 The time step

The integration of the orbit is an essential first step in computing its dimension. Besides the abovementioned total number of points of the orbit, the time step Δt with which the coordinates are advanced is another important parameter in order to compute a correct value of D. First, if Δt were too small, it would make the points to be too close to one another; this in turn would make them to be biased towards dimension 1, because there are too many points aligned along a curve; furthermore, this alignment will recur each time the orbit enters the hypersphere. This can be avoided by simply discarding neighbouring points, but this renders the small time step useless. Better off is to take a larger time step. On the other hand, Δt should not be too large: besides the longer times of integration needed to get the desired number of points of the orbit, it may yield an insufficient number of close points in order to render a meaningful correlation integral at short distances. Thus, Δt must be judiciously chosen. It is clear that a fixed value is useless, because each orbit has its own orbital period and visits the phase space at its own rate; a time step good enough to achieve a fair sample of points of a given orbit into every hypersphere, may be bad for another orbit. Therefore, it is better to fix the time step as, for example, a given fraction of the orbital period $T_{\rm p}$. This was implemented by the following procedure. First, we locate the coordinate origin at the baricenter of the density distribution. Then, we integrate the orbit with an (initially small) arbitrary time step and, by counting coordinate planes crossings, estimate its period. The integration is then started again, now taking as a time step a given fraction of this estimated period. This algorithm works fine for regular orbits, which have a definite period. Chaotic orbits, on the other hand, lack in general a definite dynamical period. Nevertheless, since the aim is to get orbital points not too close and not to far to one another, the abovementioned procedure still works even in the case of a not well-defined period, as long as the time step is chosen based on an enough number of plane crossings so that a mean time of return to the same octant can be computed.

Fig 10 shows several curves $C(r)$ corresponding to the z–tube orbit, computed using different time steps; there are also two straight lines with slopes $m = 1$ and $m = 3$ for reference. As expected, a very small Δt makes the slope to give $D = 1$ at short distances. The correct value of D is obtained just when $\Delta t \simeq 0.3 T_{\rm p}$,

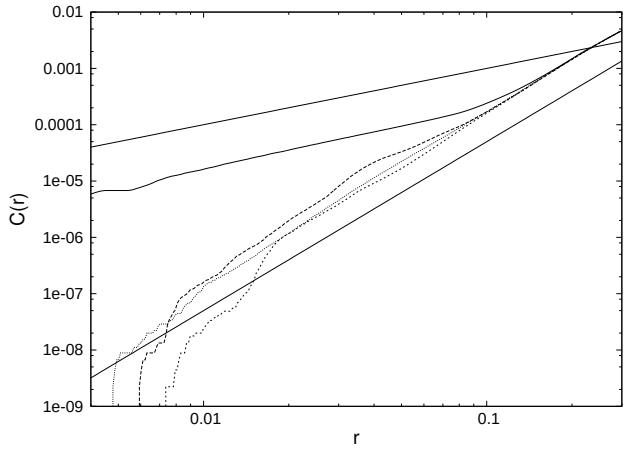

Figure 10. Correlation integral computed using different time steps. Two straight lines of slopes 1 and 3 have been added for reference. Solid line: $\Delta t = 0.0003T_{\rm p}$; long-dashed line: $\Delta t = 0.003T_{\rm p}$; short-dashed line: $\Delta t = 0.03T_{\rm p}$; dotted line: $\Delta t = 0.3T_{\rm p}$.

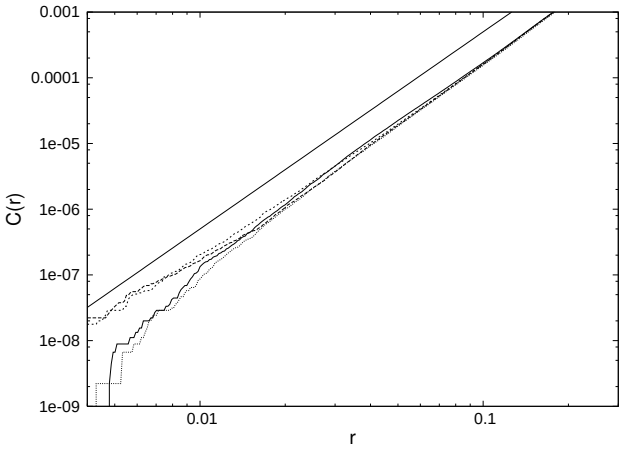

Figure 11. Correlation integral of the z–tube orbit, computed using different values of ε. A straight line of slope 3 has been added for reference. Dotted line: $\varepsilon = 8 \times 10^{-3}$, short-dashed line: $\varepsilon = 8 \times 10^{-4}$, long-dashed line: $\varepsilon = 8 \times 10^{-5}$, solid line: $\varepsilon = 8 \times 10^{-6}$.

i.e., a considerable fraction of the orbital period. Larger time steps do not appreciably improve the result, and, moreover, the integration becomes very difficult to carry out. We have found in practice that $\Delta t = 0.3T_{\rm p}$ is a good choice.

Ideally, the time step should be further scaled proportionally to the diameter of the volume of phase space visited by the orbit, to assure a well distributed sea of points and therefore a well defined $C(r)$ at all distances. This was also tried, but no appreciably improvements were observed by taking into account this correction.

3.4 The precision of the integration

The precision with which the integration of the orbit is performed has also an influence in the outcome. Let $\varepsilon \equiv |E_{\rm f} - E_0|/|E_0|$ the relative energy error in integrating the orbit, where E_0 and $E_{\rm f}$ are the energies per unit mass of the orbit at the start and at the end of the integration, respectively. Fig. 11 shows how this parameter shifts the curve $C(r)$ of the z–tube orbit at small values of r. In general, we have found that, whereas $\varepsilon \approx 10^{-5}$ or better, the function $C(r)$ maintains a correct slope. Overall, the needed precision seems not to be too demanding; a limit value of $\varepsilon = 10^{-5}$ has been adopted.

3.5 The normalization of the phase space

The normalization δ of the distance in the phase space is the factor that should be introduced in computing a Cartesian distance d between two phase space points, due to the different nature of the positions and the velocities:

$$d = \sqrt{x^2 + y^2 + z^2 + \delta^2(v_x^2 + v_y^2 + v_z^2)}. \qquad (3)$$

Since we are dealing with a correlation of distances in phase space, this factor could be very important. We have tried several possible functional forms of δ. Fig. 12 shows the result of applying to the z–tube orbit the normalization

$$\delta = \sqrt{\frac{\sigma_x^2}{\sigma_v^2}}, \qquad (4)$$

where σ_x and σ_v are the dispersions in position and velocity of the points of the orbit, respectively. This value is used in an attempt

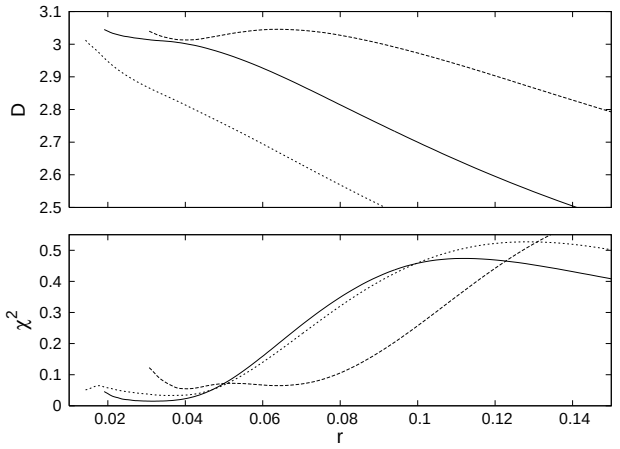

Figure 12. Top: Slopes of the different portions one decade long of the correlation integral of the z–tube orbit when computed with $\delta = \sigma_x/\sigma_v$ (long dashed curve), $\delta = 1$ (solid curve), and $\delta = \sigma_v/\sigma_x$ (short dashed curve). Bottom: errors associated with them.

to mitigate any differences between the numerical values of both positions and velocities. It is also shown in the figure the outcome when using the reciprocal of the abovementioned value of δ, in order to try to emphasize any underlying effect produced by the different nature of positions and velocities, and also it is shown the result when no normalization ($\delta = 1$) is used at all. Although it is clear that the normalization indeed affects the results, the best result, surprisingly enough, is obtained without any normalization at all. We have found that this is, in general, the case: almost always the lack of normalizaton yields the best slopes.

We reproduced the experiment shown in Fig. 2, but using the numerical values found along this section. Fig. 13 shows the result. As can be seen, almost all orbits now pile up around $D = 3$. A few orbits, however, are still far from $D = 3$. Some of them can be made $D = 3$ orbits by increasing $N_{\rm p}$; some others by increasing Δt. This shows a fundamental limitation of the method: as in the case of the computation of Lyapunov exponents, there are orbits that demand very long integration times in order to be correctly classified.

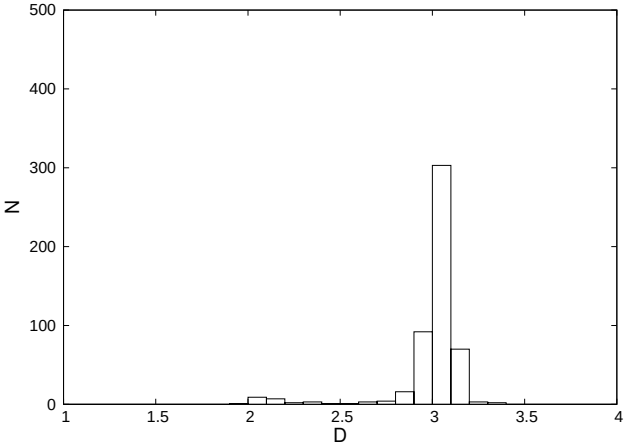

Figure 13. Same as Fig. 2, but using the numerical values of the parameters analysed in the text.

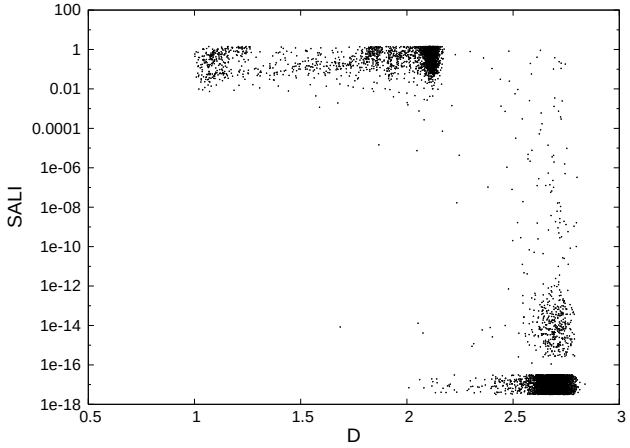

Figure 15. Comparison between the values obtained with the correlation integral and the SALI, for the sample of orbits of Fig. 14.

Table 2. Comparison of different values of the parameters of the correlation integral method, using orbits integrated in the Hénon–Heiles potential, and the SALI as a gauge. In each row, the value of the corresponding parameter is shifted, while mantaining the value of the other two at their preferred (middle) values.

Parameter	Percentages of coincidence		
$N_{\rm p} = 10^4, 3\times10^4, 5\times10^4$	92.0	97.1	97.8
$\Delta t = 0.1, 0.3, 0.5$	91.8	97.1	97.9
$\varepsilon = 10^{-4}, 10^{-5}, 10^{-6}$	97.0	97.1	97.3

Having established acceptable values of the main parameters in the case of an integrable 3D potential, there remains the issue of verifying that those values are indeed good enough when applied to other cases: 2D potentials, non integrable potentials, or both. We therefore computed the dimensions of a set of orbits integrated in the 2D, non integrable Hénon–Heiles potential (Hénon & Heiles 1964)

$$\Phi_{\rm H} = \frac{1}{2}\left(x^2 + y^2 + 2x^2y - \frac{2}{3}y^3\right) \tag{5}$$

at an energy $E = 0.125$, varying the foregoing parameters, using the results obtained with the SALI indicator (Skokos et al. 2004) as a gauge. In this last case, we integrated the orbits until $t = 1000$ units, and considered an orbit as regular whenever SALI$> 10^{-2}$, and chaotic otherwise. Table 2 shows the percentages of coincidence between both techniques. It is clear that the chosen values of the parameters of the correlation integral (middle values) suffice to obtain good results; the improvements achieved by shifting the values of the parameters towards better outputs are negligible and at an expensive cost in numerical work. Instead, shifting the parameters to the other end do have influence in the output. We conclude that the proposed values of the parameters used in obtaining the correlation integral are good enough also in cases of potentials that include chaotic regions.

4 EXPERIMENTS AND RESULTS

We have applied the method to several 2D and 3D potentials previously studied in the literature. Starting from 2D, Fig. 14 shows the $(x = 0, y, v_x > 0, v_y)$ surface of section of the Hénon-Heiles potential (Eq. (5)) at an energy $E = 0.125$, computed both by means of the correlation integral (left) and by the SALI (right). In the first case, regular orbits with $D = 1$ and $D = 2$ are shown with different symbols. In the last case, we have integrated the orbits until $t = 5000$ units and we have taken again the value SALI$= 10^{-2}$ as the bounday between regular and chaotic regimes. Each symbol in the figure indicates the computed dimension of an orbit, the initial conditions of which are the position (y, v_y) of the symbol in the plane, $x = 0$, and the positive value of v_x needed to yield $E = 0.125$. The classification of the orbits as regular or chaotic is essentially the same in both methods, except for a few orbits. Fig. 15 shows the actual values of D and SALI obtained for the complete set of analised orbits; values of SALI$= 0$ were arbitrarily distributed around $\log_{10}$SALI$= -17$ in order to visualize them in the logarithmic scale. It can be seen that, although most orbits are clearly separated by both methods, there is a set of them that received opposite classifications. We found that the number of orbits that are in this condition depends on the chosen parameters of both methods: mainly $N_{\rm p}$ and Δt for the correlation integral, and the boundary value of SALI plus the final time of integration in the case of the SALI algorithm. Regular orbits, on the other hand, have a suspicious distribution according to the correlation integral; it is not probable at all that closed orbits are clustered in that manner. Fig. 16 shows a typical orbit inside one of the $D = 1$ islands of Fig. 14 obtained with the correlation integral: it is clear that this method is not able to distinguish between this kind of slim $2D$ orbit and a real $1D$ orbit. It is worth noticing that the few regular orbits detected inside the $3D$ sea by the SALI are classified as $D = 1$ by the correlation integral. Fig. 17 shows one of them; as before, it is a very narrow orbit seen as $1D$ by the correlation integral.

We also have classified orbits in the 2D logarithmic potential

$$\Phi_{\rm L} = \frac{v_0^2}{2}\ln\left(R_{\rm c}^2 + x^2 + \frac{y^2}{q^2}\right), \tag{6}$$

where v_0, $R_{\rm c}$ and q are constants. Fig. 18 shows the $(x = 0, y, v_x > 0, v_y)$ surface of section of the logaritmic potential with $v_0 = 1$, $R_{\rm c} = 0$, and $q = 0.7$, at an energy $E = 0$ (a value that in an $R_{\rm c} = 0$, scale free potential, is arbitrary). This can be compared with Fig. 1 of Miralda Escudé & Schwarzschild (1989) and Fig. 16 of Carpintero & Aguilar (1998), where the orbits were classified using spectral dynamics. There is an interesting result here: the regions corresponding to chaotic orbits are filled with or-

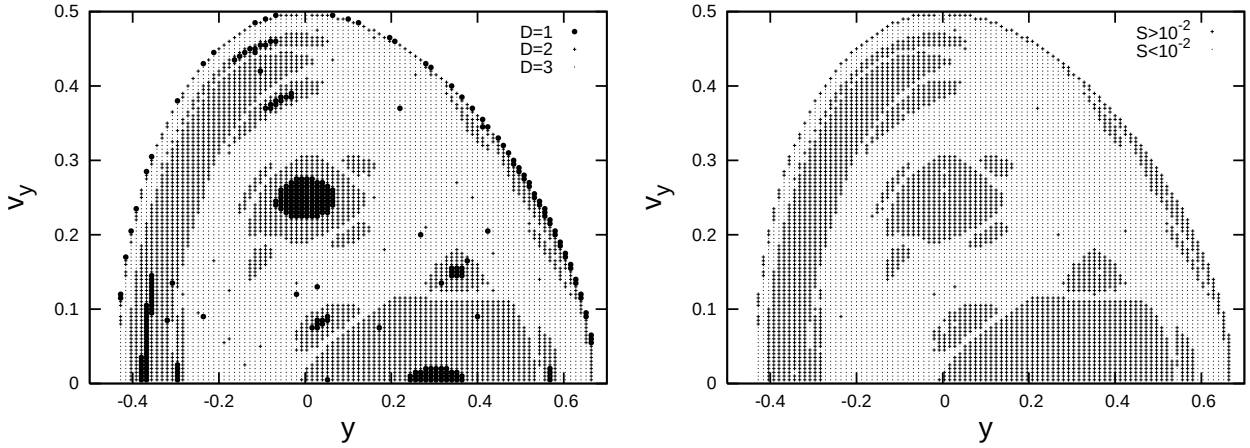

Figure 14. Surface of section of the Hénon–Heiles potential at $E = 0.125$, computed using the correlation integral (left) and the SALI (right). Each symbol represents the initial point of an orbit that was integrated and classified separately.

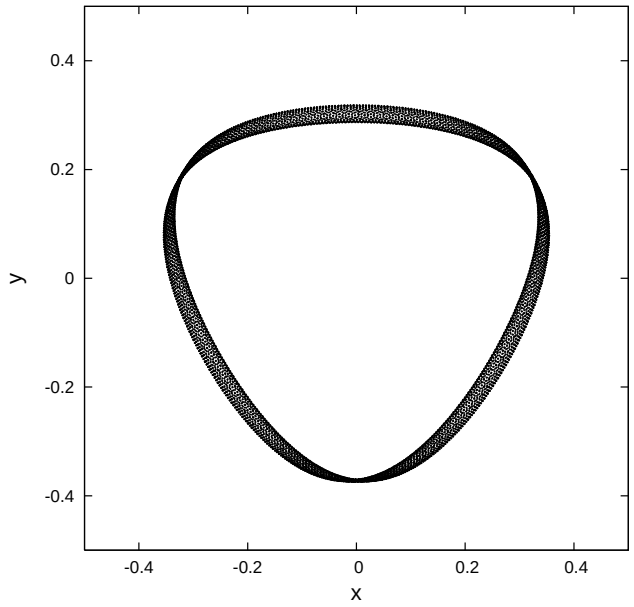

Figure 16. Orbit integrated in the Hénon-Heiles potential with initial conditions $x = 0, y = 0.304, v_y = 0.05$ and v_x so that $E = 0.125$.

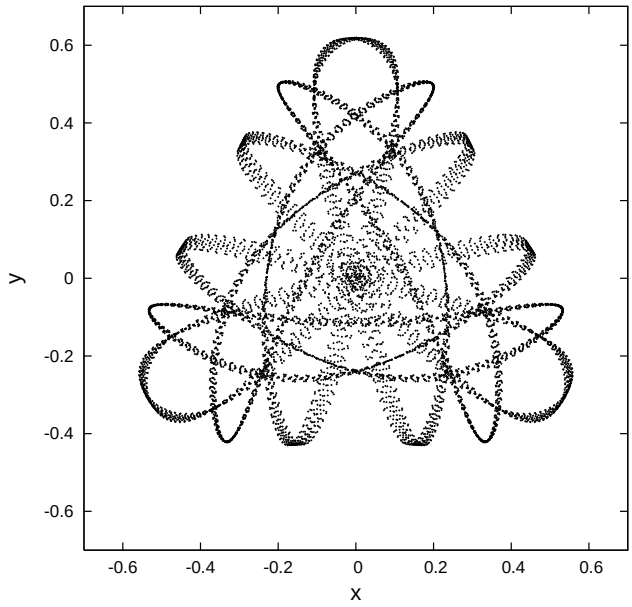

Figure 17. Orbit integrated in the Hénon-Heiles potential with initial conditions $x = 0, y = -0.02, v_y = 0.12$ and v_x so that $E = 0.125$.

bits that, according to the results of the correlation integral, move on a manifold of dimension $D = 2.4$, or, equivalently, they obey 1.6 isolating integrals of motion! This of course cannot be true. We isolated one of these orbits, and studied it in detail, in order to find out the origin of this behaviour. Fig. 19 shows two portions of this orbit, selected at different time intervals. The upper panel shows an ordinary regular orbit, whereas the lower panel shows that the orbit is transiting between different regular regimes. The corresponding correlation integrals are shown in Fig. 20. The orbit is effectively a regular orbit during the first stage ($D = 2$), but its correlation integral takes a slope $D = 2.6$ during the second interval. These regimes were the only two found along any investigated portion of the orbit. The intervals in which the slope takes the value $D = 2.6$ are those in which the orbit is merely transiting between different regular regimes. The histograms of the correlation integral of the regular parts plus those of the transiting parts add up to yield the final $D = 2.4$ figure. That is, the orbit never moves in a 3D manifold, nor it moves permanently in a 2D manifold. Fig. 21 shows, for this orbit, the evolution of its positive Lyapunovs exponents and of the SALI. Here, and in the rest of this work, Lyapunov exponents were computed using a Gram-Schmidt orthogonalization of four displacement vectors every time step, renormalizing at the same time the vectors, following the recipe of Bennetin et al. (1980). In order to determine the threshold value between regular and chaotic regimes, we followed the recipe of Carpintero et al. (2003). Both Lyapunov exponents and SALI find this orbit chaotic, illustrating the fact that it is not moving at all times in a fixed 2D manifold. This last statement is corroborated in Fig. 16 of Carpintero & Aguilar (1998), in which all these orbits with slopes $D \simeq 2.4$ in their correlation integrals were classified as irregular by the spectral dynamics. Moreover, as shown in Figs. 22 and 23, all these orbits are classified as chaotic according to their Lyapunov exponents or SALI values, i.e., they all show sensitivity to the initial conditions. Therefore, we have here a numerical proof that, in a 2D potential,

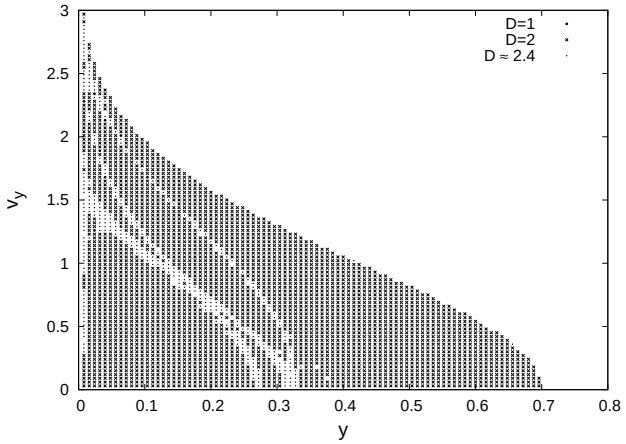

Figure 18. Same as Fig. 14, but for the logarithmic potential at $E = 0$.

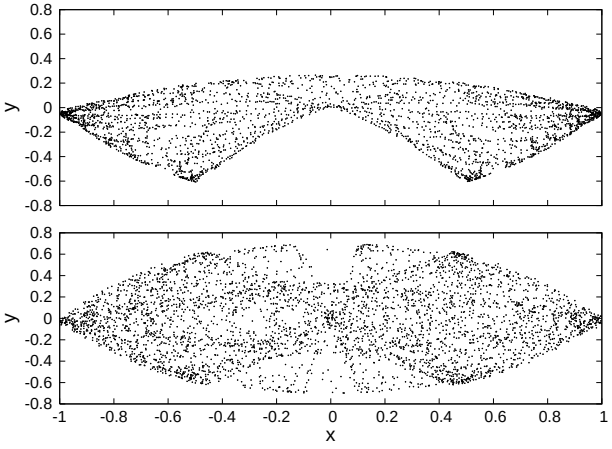

Figure 19. Two different time intervals of the same orbit integrated in the logarithmic potential. The upper panel, between $t = 2598$ and $t = 6785$, shows that the orbit is completely regular in this interval. The lower panel, between $t = 40421$ and $t = 46195$, shows the orbit transiting between three regular regimes.

a chaotic orbit (defined as having sensitivity to the initial conditions) or a 2D irregular orbit (defined as not being regular) is not neccesarily an orbit that moves in a manifold of dimension 3.

We also classified orbits in the Binney potential (Binney 1982)

$$\Phi_{\rm B} = \frac{v_0^2}{2} \ln \left[R_{\rm c}^2 + x^2 + \frac{y^2}{q^2} - \frac{(x^2+y^2)^{1/2}(x^2-y^2)}{R_{\rm e}} \right], \quad (7)$$

where v_0, q, $R_{\rm c}$ and $R_{\rm e}$ are constants. Fig. 24 shows the $(x, y = 0, v_x, v_y > 0)$ surface of section of this potential, with $v_0 = 1$, $q = 0.9$, $R_{\rm c} = 0.14$ and $R_{\rm e} = 3$, at an energy $E = -0.4641$. This figure may be compared with Figs. 3.41 and 3.42 of Binney & Tremaine (2008), where several orbits puncturing this surface of section are showed; the chaotic sea and the regular regions and islands are well reproduced. The two regions of $D = 1$ orbits are composed, again, of orbits near closeness, which the correlation integral sees as unidimensional.

We have also classified a set of 3472 orbits previously analised by Muzzio, Carpintero & Wachlin (2005), integrated in an analytical potential obtained from a cold collapse of 100,000 particles (see Muzzio, Carpintero & Wachlin (2005) for details). They classified the orbits by computing their Lyapunov exponents, and the result-

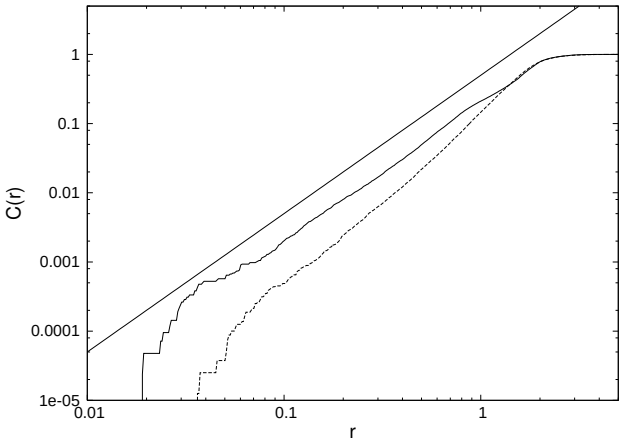

Figure 20. Correlation integrals of the portions of orbit shown in Fig. 19. Solid line: first interval; dashed line: second interval. A straight line of slope 2 is plotted for reference.

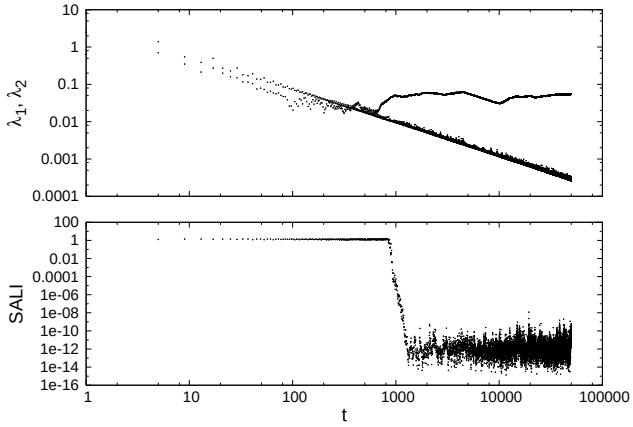

Figure 21. Positive Lyapunov exponents and the SALI of the orbit shown in Fig. 19. The first episode of irregularity occurs near $t = 750$, which is the transition detected by both methods.

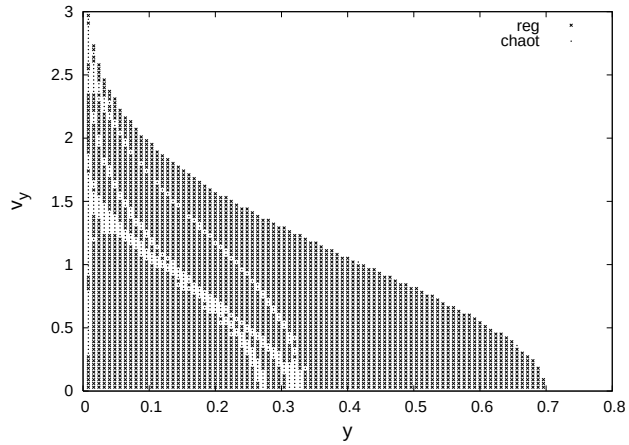

Figure 22. Same as Fig. 18, but computing the chaoticity with Lyapunov exponents. All the orbits were integrated until $t = 10,000$.

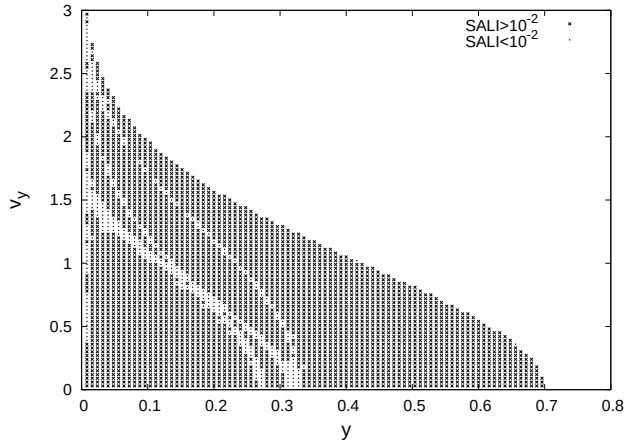

Figure 23. Same as Fig. 18, but computing the chaoticity with the SALI. The threshold value was chosen at SALI$= 10^{-2}$. All the orbits were integrated until $t = 5,000$.

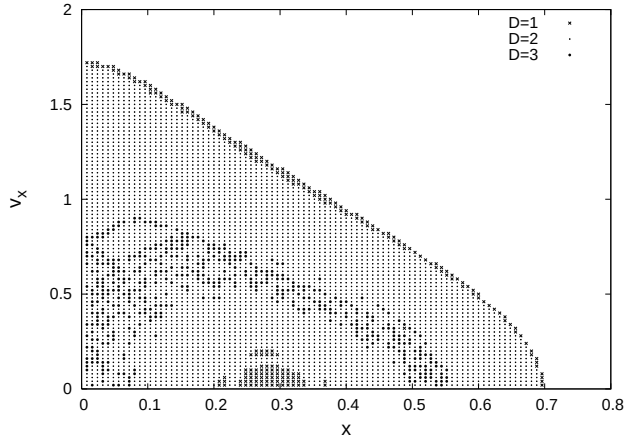

Figure 24. Orbital content of the Binney potential with $v_0 = 1$, $q = 0.9$, $R_{\rm c} = 0.14$ and $R_{\rm e} = 3$, at an energy $E = -0.4641$.

ing regular ones were further classified by means of the spectral dynamics. The dimension obtained with the correlation integral was rounded to the nearest integer in order to compare both methods. Table 3 shows the results.

Inspecting the table, it is quite clear that the results are not the same in both classifications. In order to quantify this, we performed a crosstabulation analysis (Press et al. 1994), using Table 3 as a contingency table. Using Sakoda's adjusted Contingency Coefficient V as an indicator of the strength of association between the results of both methods, the value obtained was $V = 0.48$, an

Table 3. Comparison between the dimension of the manifold obtained using Lyapunov exponents plus spectral dynamics (rows) and using the correlation integral (columns), for 3472 orbits integrated in the potential described in Muzzio, Carpintero & Wachlin (2005).

D	1	2	3	4	5
1	0	0	0	0	0
2	0	10	78	2	1
3	0	137	1406	6	4
4	0	11	235	38	29
5	0	8	236	214	1057

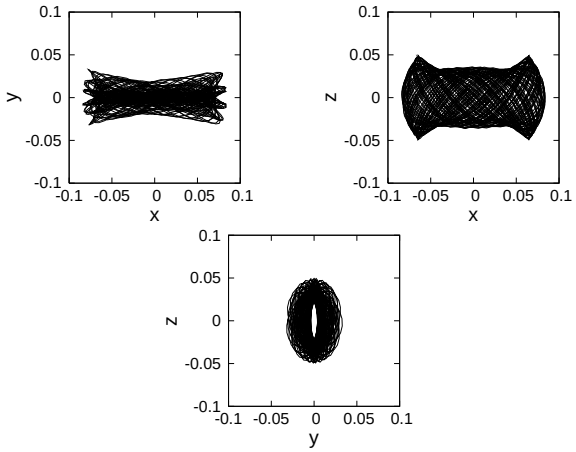

Figure 25. Example orbit in configuration space.

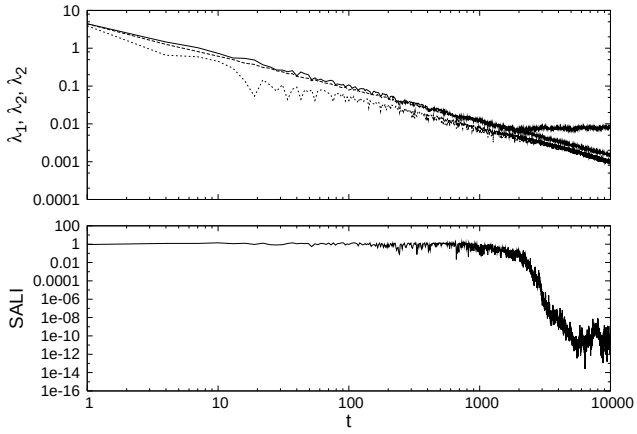

Figure 26. The three positive Lyapunov exponents and the SALI, as a function of time, corresponding to the orbit of Fig. 25.

intermediate value of correlation. To measure the significance of this figure, we performed a χ^2 test, resulting in the probability of obtaining by chance our value of $\chi^2 = 2392.4$ with 9 degrees of freedom (note the null row and the null column) being less than 10^{-6}, i.e., the value of the correlation $V = 0.48$ is indeed statistically significant, and therefore the classifications indeed differ one another. Other indicators of association gave similar results.

We analysed in detail a randomly chosen orbit that had different dimensions according to both methods. Fig. 25 shows the chosen orbit in configuration space. According to the correlation integral, this orbit moves in a manifold of dimension $D = 3$ (a regular orbit), but its Lyapunov exponents render it as a partially chaotic orbit, i.e., $D = 4$, as shown in the upper panel of Fig. 26. On the other hand, the spectral analysis, besides finding that it is an x–tube orbit, yielded $D = 3$. (We recall that only those orbits classified as regular by their Lyapunov exponents were further classified using the spectral dynamics; thus, this orbit appears in the table with $D = 4$ and not with the $D = 3$ that the last method would have assigned to it.) Also, the lower panel of Fig. 26 shows that, although the value of the SALI does not tend to the numerical zero ($\simeq 10^{-16}$ in our double precision experiments), it does have an enough low value to allow classifying the orbit as chaotic. Visually inspecting Fig. 25, it appears to be indeed a regular orbit; however, a closer inpection reveals a slight dishevelled aspect, which is in

Table 4. Expected and computed behaviours of the GALI_k indices.

	Expected if $D = 2$	Expected if $D = 3$	Computed
$\mathrm{GALI}_2 \propto$	t^0	t^0	t^0
$\mathrm{GALI}_3 \propto$	t^{-1}	t^0	t^0
$\mathrm{GALI}_4 \propto$	t^{-2}	t^{-2}	t^0
$\mathrm{GALI}_5 \propto$	t^{-4}	t^{-4}	t^{-1}
$\mathrm{GALI}_6 \propto$	t^{-6}	t^{-6}	t^{-2}

general the signature of a sticky orbit, i.e., an orbit that is irregular but that wanders during a long time close to a regular torus. This result shows the limitations of the correlation integral to cope with sticky orbits. On the other hand, sticky orbits may remain confined to a definite volume of the phase space during large periods of time, therefore lacking the characteristic diffusion of other chaotic orbits through phase space that may greatly influence the global dynamics of an entire stellar system. If the period of stickiness is larger than the period of interest, the sticky orbit can be considered effectively regular, as the correlation integral and the spectral dynamics do; in other circumstances, it should be classified as chaotic, as the Lyapunov exponents or the SALI do. This analysis enhances the fact that in order to understand the nature of some difficult orbits we should combine information from several techniques.

We have examined some other orbits with $D = 3$ according to the correlation integral, and with $D > 3$ according to the Lyapunov exponents. Most of them followed the same pattern as the last example; however, in a few cases, the orbits were clearly irregular, and therefore correctly classified by the Lyapunov exponents; the SALI classified these orbits as chaotic in all the cases. Orbits with $D = 4$ according to one method and $D = 5$ according to the other were not analized, because their true dimensions cannot be asserted visually nor in other independent ways.

With respect to the regular orbits, a possible source of the differences between classifications might be the rounding of the dimension obtained with the correlation integral to the nearest integer. We shifted the limit between integers, and found that, for example, varying the boundary between orbits with $D = 2$ and with $D = 3$ in the interval $D \in [2.3, 2.7]$ barely improves the coincidence with the classification of the spectral dynamics. We therefore took one $D = 2$ orbit according to the correlation integral, but classified $D = 3$ by the spectral dynamics, and computed its GALI_k indices in order to determine its dimension. We expect GALI_k behave as indicated in the second and third columns of Table 4 if the orbit moves on a 2D or 3D torus, respectively (Skokos, Bountis & Antonopoulos 2008). The left panel of Fig. 27 shows the computed values of the GALI_k indices for this orbit; the fourth column of Table 4 reproduces this result in terms of powers ot time. As can be seen, the behaviour is not what one would expect. A similar analysis using another orbit for which the correlation integral yielded $D = 3$ but classified as $D = 2$ by the spectral dynamics gave exactly the same behaviour in its GALI_k indices (Fig. 27, right panel). There is the possibility that one or more of our initial deviation vectors to compute the indices were tangent to the respective tori. But, even in this case, the expected power laws (Skokos, Bountis & Antonopoulos 2007) would not coincide with those computed. Evidently, this result deserves a deeper study, but which is beyond the scope of this work.

Therefore, we turn to a visual inspection of some of these orbits. Although we found, as was the case with the chaotic orbits, that there were a few orbits misclassified by the correlation integral that were correctly classified by the spectral dynamics, we found

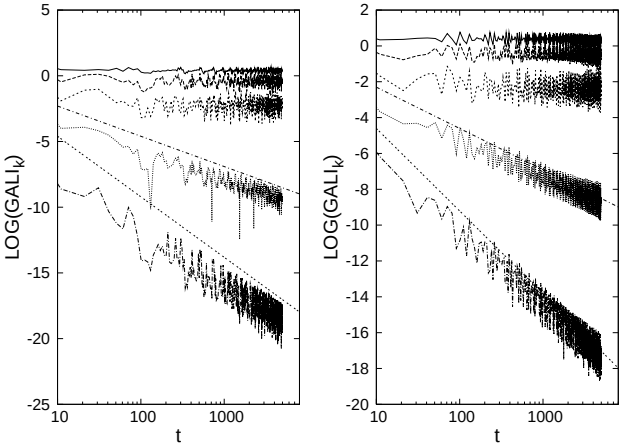

Figure 27. $\mathrm{GALI}_k(t)$ for the example orbits. From top to bottom: GALI_2, GALI_3, GALI_4, GALI_5 and GALI_6. The straight lines have slopes -1 and -2.

that most of them seemed to have the dimension given by the correlation integral. When examining their Fourier spectra to find out why the spectral dynamics method assigned these orbits a wrong dimension, we found that those spectra had close lines, which is the single most important numerical problem of the spectral dynamics.

5 CONCLUSIONS

We have analized a method to find the dimension of the manifold on which an orbit moves, dubbed the correlation integral. This amounts to find out how many isolating integrals of motion the orbit has. In turn, this last number allows to classify the orbit as regular or chaotic, and, among these two categories, whether it is closed or resonant, of whether it is partially or fully chaotic. The method turns out to be easy to implement, but it depends on a number of numerical parameters which have to be chosen with some care in order to obtain good results. We have analized the most important parameters, finding the numerical values that allow the method to be reliable.

The method was applied to orbits integrated in a Stäckel potential, obtaining that most of them move in a manifold of dimension 3, as expected. However, a few orbits with computed dimensions below 3 can be well classified provided that they are integrated during longer times, as is the case of the computation of chaoticity by means of Lyapunov exponents. The method was also applied to a number of other potentials previously studied in the literature, and compared against other gauges of chaoticity and/or regularity (Lyapunov exponents, SALI/GALI and spectral dynamics), giving in general satisfactory results. Detailed analyses of the orbits that were variously classified by the different methods showed a limitation of the correlation integral, in particular to cope with near closed orbits, for which $D = 1$ is obtained instead of the correct $D = 2$, and sticky orbits, which are already difficult to cope with for any algorithm intending to classify them. As said before, these results expose the need of combininig information from several techniques before a conclusive answer could be given for any particular orbit. For chaotic orbits, in particular, it was found that the Lyapunov exponents may not give the true dimension of the manifold on which the orbit moves. The fact that the exponential divergence may not be a direct measure of the dimension of the manifold of the trajectory was already proved for maps (see, e.g.,

Jackson 1991, §4.6). The experiments described here show that this may be true also for continuous differential equations.

A FORTRAN 77 program that computes the correlation integral is freely available upon request.

ACKNOWLEDGMENTS

We would like to thank the referee for very useful comments which allowed to improve the paper. This work was supported by grants of the Universidad Nacional de La Plata, the Consejo Nacional de Investigaciones Científicas y Tecnológicas, and the Agencia Nacional de Promoción Científica y Tecnológica de la República Argentina.

REFERENCES

Arnold V.I., 1989, Mathematical Methods of Classical Mechanics, Springer-Verlag, New York
Barnes E.I., 2001, ApJ, 559, 736
Bennetin G., Galgani G., Giorgilli A., Strelcyn J.M., 1980, Meccanica, 15, 9
Binney J., 1982, MNRAS, 201, 1
Binney J., Spergel D., 1982, ApJ, 252, 308
Binney J., Tremaine S., 2008, Galactic Dynamics, 2nd Edition, Princeton Univ. Press, Princeton
Carnevali P., Santangelo P., 1984, ApJ, 281, 473
Carpintero D.D., Aguilar L.A., 1998, MNRAS, 298, 1
Carpintero D.D., Muzzio J.C., Vergne M.M., Wachlin F.C., 2003, Cel. Mech. & Dyn. Ast., 85, 247
Contopoulos G., 1983, A&A, 117, 89
Cretton N., Rix H.-W., de Zeeuw P., 2000, ApJ, 536, 319
de Zeeuw P., 1985, MNRAS, 216, 273
Ding M., Grebogi C., Ott E., Sauer T., Yorke J.A., 1993, Phys. Rev. Letters, 70, 3872
Dvořák I., Klaschka J., 1990, Phys. Let. A, 145, 225
Grassberger P., Procaccia I., 1983, Phys. Rev. Letters, 50, 346
Heinämäki P., Lehto H.J., Valtonen M.J., Chernin A.D., 1998, MNRAS, 298, 790
Hénon M., Heiles C., 1964, AJ, 69, 73
Jackson E.A., 1991, Perspectives of nonlinear dynamics, Cambridge Univ. Press, Cambridge
Kantz H., Schreiber T., 1997, Nonlinear Time Series Analysis, Cambridge Univ. Press, Cambridge
Laskar J., 1990, Icarus, 88, 266
Merritt D., Fridman T., 1996, ApJ, 460, 136
Miralda Escudé J., Schwarzschild M., 1989, ApJ, 339, 752
Muzzio J.C., 2003, Bol. Asoc. Argentina Astron., 45, 69
Muzzio J.C., Mosquera M.E., 2004, Cel. Mech. & Dyn. Ast., 88, 379
Muzzio J.C., Carpintero D.D., Wachlin F.C., 2005, Cel. Mech. & Dyn. Ast., 91, 173
Press W.H., Teukolsky S.A., Vetterling W.T., Flannery B.P., 1994, Numerical Recipes in FORTRAN, 2nd edition, Cambridge Univ. Press, Cambridge
Schwarzschild M., 1979, ApJ, 232, 236
Schwarzschild M., 1982, ApJ, 263, 599
Skokos Ch., Antonopoulos Ch., Bountis T.C., Vrahatis M.N., 2004, J. Phys. A: Math. Gen., 37, 6269
Skokos Ch., Bountis T.C., Antonopoulos Ch., 2007, Physica D, 231, 30
Skokos Ch., Bountis T.C., Antonopoulos Ch., 2008, arXiv:0802.1646 nlin.CD
Valluri M., Merritt D., ApJ, 506, 686
Voglis N., Kalapotharakos C., Stavropoulos I., 2002, MNRAS, 337, 619